HHS Public Access

Author manuscript

Brain Stimul. Author manuscript; available in PMC 2023 December 07.

Published in final edited form as:

Brain Stimul. 2023 ; 16(5): 1430–1444. doi:10.1016/j.brs.2023.09.013.

Disrupting nociceptive information processing flow through transcranial focused ultrasound neuromodulation of thalamic nuclei

Arabinda Mishra[a,b], **Pai-Feng Yang**[a,b], **Thomas J. Manuel**[a,c], **Allen T. Newton**[a,b], **M. Anthony Phipps**[a], **Huiwen Luo**[a], **Michelle K. Sigona**[a], **Jamie L. Reed**[a], **John C. Gore**[a,b,c], **William A. Grissom**[a,c], **Charles F. Caskey**[a,b], **Li Min Chen**[a,b,c,*]

[a]Vanderbilt University Institute of Imaging Science, Vanderbilt University, Nashville, TN, USA

[b]Department of Radiology and Radiological Sciences, Vanderbilt University Medical Center, Nashville, TN, USA

[c]Department of Biomedical Engineering, Vanderbilt University, Nashville, TN, USA

Abstract

Background: MRI-guided transcranial focused ultrasound (MRgFUS) as a next-generation neuromodulation tool can precisely target and stimulate deep brain regions with high spatial selectivity. Combined with MR-ARFI (acoustic radiation force imaging) and using fMRI BOLD signal as functional readouts, our previous studies have shown that low-intensity FUS can excite or suppress neural activity in the somatosensory cortex.

Objective: To investigate whether low-intensity FUS can suppress nociceptive heat stimulation-induced responses in thalamic nuclei during hand stimulation, and to determine how this suppression influences the information processing flow within nociception networks.

Findings: BOLD fMRI activations evoked by 47.5 °C heat stimulation of hand were detected in 24 cortical regions, which belong to sensory, affective, and cognitive nociceptive networks. Concurrent delivery of low-intensity FUS pulses (650 kHz, 550 kPa) to the predefined heat

*Corresponding author. Department of Radiology and Radiological Sciences, Institute of Imaging Science, Vanderbilt University Medical Center, AA 1105 MCN 1161 21st Ave. S., Nashville, TN 37232, USA. limin.chen@vanderbilt.edu (L.M. Chen).

Authors contribution

Arabinda Mishra: Analyzed fMRI data, wrote the first draft of the manuscript, and edited the final manuscript. Pai-Feng Yang: Participated in data acquisition and animal care. Thomas J Manuel: FUS-fMRI and MR-ARFI data collection and analysis. Allen T Newton: Participated in the data acquisition. M. Anthony Phipps: Participated in FUS-fMRI and MR-ARFI data collection and analysis and wrote part of the manuscript. Huiwen Luo: Developed and optimized MR-ARFI data acquisition protocol and analysis pipeline. Participated in data collection and analysis. Michelle K Sigona: Participated in FUS-fMRI and MR-ARFI data collection and analysis. Jamie L Reed: Assisted data collection, engaged in animal care, and edited the manuscript. John C Gore: Provided conceptual guidance on MRI data acquisition and edited manuscript. William A Grissom: Designed MR-ARFI experiment, supervised MR-ARFI data acquisition, interpreted MR-ARFI maps, and edited manuscript. Charles F Caskey: Designed FUS experiment, supervised data acquisition, interpreted MR-ARFI maps, and edited manuscript. Li Min Chen: Designed fMRI experiment, supervised FUS-fMRI data acquisition, interpreted fMRI maps wrote, and edited the manuscript.

Appendix A. Supplementary data

Supplementary data to this article can be found online at https://doi.org/10.1016/j.brs.2023.09.013.

Declaration of competing interest

The authors declare that they have no known competing financial interests or personal relationships that could have appeared to influence the work reported in this paper.

nociceptive stimulus-responsive thalamic centromedial_parafascicular (CM_para), mediodorsal (MD), ventral_lateral (VL_ and ventral_lateral_posteroventral (VLpv) nuclei suppressed their heat responses. Off-target cortical areas exhibited reduced, enhanced, or no significant fMRI signal changes, depending on the specific areas. Differentiable thalamocortical information flow during the processing of nociceptive heat input was observed, as indicated by the time to reach 10% or 30% of the heat-evoked BOLD signal peak. Suppression of thalamic heat responses significantly altered nociceptive processing flow and direction between the thalamus and cortical areas. Modulation of contralateral versus ipsilateral areas by unilateral thalamic activity differed. Signals detected in high-order cortical areas, such as dorsal frontal (DFC) and ventrolateral prefrontal (vlPFC) cortices, exhibited faster response latencies than sensory areas.

Conclusions: The concurrent delivery of FUS suppressed nociceptive heat response in thalamic nuclei and disrupted the nociceptive network. This study offers new insights into the causal functional connections within the thalamocortical networks and demonstrates the modulatory effects of low-intensity FUS on nociceptive information processing.

Keywords

Transcranial focused ultrasound; Primates; fMRI; Neuromodulation; Pain network; Hand; Somatosensory

1. Introduction

Transcranial focused ultrasound (FUS) is increasingly recognized as a next generation neuromodulation tool for dissecting brain circuits in neuroscience research and potentially as a therapeutic device in clinical practice [1]. Compared to other noninvasive neuromodulation tools such as transcranial/intracranial electrical stimulation (TES/IES) [2–4] and transcranial magnetic (TMS) [5–7], FUS takes the edge in precisely targeting deep brain structures [8,9] and also non-invasively stimulate millimeter-scale brain regions having higher spatial selectivity [10,11]. When used in conjunction with MRI, FUS can be a powerful noninvasive therapeutic tool for chronic pain management as it can be precisely localized using MR-acoustic radiation force imaging (MR-ARFI) while network-level functional modulation can be monitored with BOLD fMRI feedback [12–14]. As a neuromodulator, FUS can exert both excitatory and inhibitory effects due to its action on different ionic channels on neuron membranes [15,16]. The ability to excite and inhibit neural activity during various states of activation [17] can have significant implications on the future application of neuromodulation on various cognitive and pathological conditions [13].

Thalamus plays a critical role in pain perception, as documented in both health and chronic pain conditions. For example, anatomical tracing and electrophysiology studies in non-human primates (NHP) have identified nociceptive activity or ascending spinothalamic tracts (SST) afferents in thalamic nuclei, including ventral posterior lateral nucleus (VPL), ventral posterior inferior nucleus (VPI), central lateral nucleus (CL), medial part of the posterior complex (POm), the posterior part of the ventral medial nucleus (VMpo), mediodorsal nucleus (MD), parafascicular nuclei (Pf), midline thalamic nuclei (such as submedius nucleus (Sm)), and intralaminar thalamic nuclei (ILN) [18]. Resting-state functional connectivity analysis revealed its role as a core hub connecting to pain sub-networks [19].

Our submillimeter resolution fMRI studies have identified several thalamic nuclei that are responsive to nociceptive heat stimulation of hands in anesthetized monkeys [20], even though their links to pain perception remain to be determined. Micro-stimulation in the VP nucleus is more likely to elicit pain in Central Post-Stroke Pain (CPSP) patients than in non-stroke, non-pain patients [21]. It can also induce phantom sensations, including pain, in amputees [22]. In stroke patients, inferolateral territory infarction, which disrupts irrigation of VP and VL nuclei, induces sensory loss and CPSP [23]. DBS neuromodulation or ablation (i.e., thalamotomy) of the thalamic ventral caudal (VC) nucleus has shown pain relief in many chronic pain conditions including post-stroke pain, phantom pain, and cancer pain (for recent reviews [24–26]). The specific roles of different thalamic nuclei in pain are not fully understood, partly due to the lack of non-invasive tools that allow both precise modulation and comparative assessment of different thalamic targets. FUS holds tremendous potential for the accurate stimulation of various deep brain structures, including thalamic nuclei, and for investigating their direct involvement in pain. As a demonstration of the potential of FUS in pain management, a recent study has reported that FUS stimulation of the anterior thalamic nucleus altered the pain detection threshold in healthy subjects [9].

Our team has successfully developed an MR-guided FUS system with fMRI monitoring in recent years. We have previously shown that FUS can either activate or suppress neural activity engaged in processing innocuous tactile information in the primary somatosensory cortex areas 3a/3b in a brain state-dependent manner by fMRI [13,14,27]. In this study, our aim is to determine whether FUS can suppress thalamic neural responses evoked by nociceptive heat stimulation, using FUS parameters known to induce inhibitory effects in the somatosensory cortex of NHPs [13]. We anticipate that these findings will establish a foundation for employing FUS neuromodulation in future clinical trials targeting pain management. We then examine the consequence of thalamus suppression on the information processing flow between thalamic nucleus and off-target cortical regions during nociceptive heat versus heat plus concurrent FUS stimulation. Moreover, MRgFUS offers a novel way to dissect pain networks and probe the causal relationships between important pain hubs and brain networks. Consequently, FUS can be utilized to accurately identify targets for intervention. Additionally, FUS has potential as a non-invasive pain management tool, allowing for targeted therapy to specific brain regions on a scheduled basis. By conducting simultaneous FUS and fMRI studies, researchers can gain insights into the role of thalamic nuclei and their casual and functional connections with other nociceptive regions in the NHP brain. As a robust model, this approach can pave the way for optimizing FUS protocols to facilitate target identification for pain therapy and improve our understanding of human pain networks.

The NHP brain is selected as the research model due to its relatively large size, making it well-suited for establishing the methodology and optimizing the sonication dosimetry. This study employed the recently developed MRgFUS system to address the following specific questions: (1) whether the suppressive FUS pulses, previously established in the touch system, can also suppress heat nociceptive BOLD response at thalamus nuclei, (2) how the suppression of thalamic nociceptive signaling affects interconnected brain regions, and (3) whether the suppression of thalamic heat response alters the flow of nociceptive information processing within nociceptive networks.

2. Materials and methods

2.1. Animal preparation

Four adult macaque monkeys (two female *Macaca fascicularis* and two male *M. mulatta*) underwent five MRI and FUS experimental sessions. Animals were initially sedated with ketamine hydrochloride (10 mg/kg) and atropine sulfate (0.05 mg/kg) and then anesthetized with isoflurane (1.0%–1.5%) delivered in oxygen. After intubation, each animal was placed in a custom-designed MR stereotaxic frame with the head secured by ear bars, eye bars, and mouthpieces. During fMRI data acquisition, the anesthesia level was maintained around 1–1.2%, ensuring that vital signals remained very stable (heart rate:160 ± 5; end tidal CO_2: 32 ± 3, and SpO_2: 99 ± 1%). A solution of 2.5% dextrose in saline was infused intravenously (3 ml/kg/h) to prevent dehydration. Animals were artificially ventilated throughout the experiment. The body temperature was maintained by a circulating water blanket. All procedures were conducted in accordance with National Institutes of Health guidelines and were approved by the Institutional Animal Care and Use Committee of Vanderbilt University.

2.2. Peripheral nociceptive heat stimulation protocol

A custom microcontroller program coordinated pulsing for alternating heat and heat + FUS stimulation. The fingers were stabilized with a custom-built hand/finger holder, palm side up, leaving the glabrous skin of the distal finger pads available for stimulation. Nociceptive heat 47.5 °C stimuli were delivered to the fingers of the left hand via a CHEPS thermal probe (30 mm in diameter, Medoc). For each fMRI stimulation run, three stimulus conditions – FUS only, heat only, and heat + FUS (of thalamic nuclei) - were presented in interleaved 16-s duration blocks in a randomized sequence. Only heat and heat + FUS stimulation blocks were analyzed here. Each stimulation condition was repeated seven times. The thermal probes remained in contact with the skin of the fingers (at 32 °C temperature) during 30-s baseline periods between stimulation conditions (Fig. 1).

2.3. MRI data acquisition

All MRI scans were performed on a Philips 3T Ingenia CX with a pair of FLEX surface coils (inner diameter = 12 cm) positioned on both sides of the head. Three types of MR images were acquired. (1) A series of T2*-weighted whole-brain structural MR images (TE = 1.89 ms, TR = 4 ms, 400 × 400 × 140 matrix, 0.35 × 0.35 × 2 mm^3 voxel size, flip angle 10°, NSA = 1). (2) fMRI data were acquired using a single shot GE-EPI sequence (TE = 30 ms, TR = 2s, 1.43 × 1.43 × 2mm voxel size and 112 × 112 × 36 matrix size). (3) Whole-brain high-resolution T1-weighted structural image (TE = 4.6 ms, TR = 9.9 ms, 500 × 512 × 512 matrix, 0.5 × 0.49 × 0.49 mm^3 voxel size and flip angle 8°). The high resolution T1-weighted were primarily used for EPI data normalization in the template space. Each fMRI run contained 337 imaging volumes. An extra navigator echo was collected with no phase encoding prior to the acquisition of the actual image data. This echo is used to correct for phase variations typically caused by motion. In a typical fMRI session, a total of 3–4 runs were acquired.

2.4. fMRI data analysis

2.4.1. Pre-processing—The standard pre-processing, including 3-D motion correction, slice timing correction, and normalization of fMRI data to the template, was performed using FSL (*mcflirt, slicetimer, flirt, fnirt*) and custom Matlab code (R2019b). Six motion parameters, along with BOLD temporal signals extracted from voxels in white matter and CSF regions that contain at least 70% of the cumulative variance (derived from principal components analysis), were considered nuisance parameters and were regressed out and the first five EPI image volumes (10 s) were eliminated. The median EPI image in each run was co-registered (affine) to the T1w anatomic image in each individual subject space. The transformation was then applied to the fMRI time series. Each subject's T1w anatomic image was then co-registered (non-rigid) with the macaque template (NMT_v2.0) [28,29], and the transformation was applied to the fMRI data for the group-level analysis. No spatial smoothing was performed before and after the normalization of the EPI data into the space. The BOLD time series were temporally filtered (Chebyseb type II) at a low-pass cutoff frequency of 0.25 Hz.

In total, 24 runs obtained from five imaging sessions in four monkeys) were analyzed. Three out of twenty-seven functional EPI runs with motion parameters >1 mm and temporal SNR <16 were excluded from the analysis. Each run was analyzed separately using GLM. For group analysis at the subject level (second level), we used a higher-level mixed-effects model. This model accounts for both within-subject variability, arising from multiple runs, and between-subject variability. In this model, repeated measures from multiple runs are treated as a random effect. To ensure that results were not influenced by any specific subject, we quantified the cycle-averaged mean percentage signal changes (PSC) and the standard deviation (SD) across runs for each subject, and then across all four subjects for each ROI. No significant differences between subjects were observed therefore all runs were included in the analysis.

2.4.2. Detection of stimulus-driven activations—To localize the stimulus-driven activation, we performed voxel-wise analyses of BOLD time courses using a generalized linear model (GLM). The stimulus paradigm convolved with the hemodynamic response function was used as a predictor to model the stimulus-driven BOLD activation. Voxels that showed stimulus-evoked changes in response to Heat or Heat + FUS (versus Rest) stimulation at a statistically significant level ($t > 2$, $p < 0.05$, FDR corrected) with a minimum of two contiguous EPI voxels were considered as activation and overlaid on the NMT template for display. Brain regions of interest (ROIs) showing above threshold activation were identified using the macaque monkey NMTv2.0 atlas. Clustering in the native space was the criterion used for identifying the activated brain regions that exhibited the most drastic changes when FUS was delivered at VPL and four surrounding thalamic nuclei.

We also created subtraction maps for two conditions (heat versus heat + FUS) to illustrate the changes in the activation maps. To generate these maps, we constructed a binary mask that excluded overlapping statistically significant voxels present in the activation maps of both stimulus conditions. The resulting differential activation map represents the ROIs and

voxels where BOLD signal changes were more associated with one stimulus condition over the other. The ROIs identified in either the heat or heat + FUS networks showed statistically significant signal increases over the resting periods. Identification of each activated cortical area was automatically annotated in the macaque atlas space using custom Matlab code and AFNI.

2.4.3. BOLD signal time course analysis—BOLD signals were extracted from each brain region of interest (ROI). Block-averaged percentage signal changes (PSC) were quantified. The mean signal 6 s (three EPI volumes) prior to the stimulus onset in each block was considered as the baseline for calculating the PSC at each time point after stimulus onset. The block-averaged mean time courses were fitted with a double gamma variate function for identifying the PSC peak. For each ROI, the peak BOLD signal change was calculated by averaging PSC within a symmetric 8-s time window around the peak time point. The times of signal rising to 10%, 30%, and 50% of the peak PSC were derived from gamma fitting curves, considering the stimulus onset as time zero. Time and PSC differences between two conditions (heat versus heat +FUS) at each ROI were statistically quantified using a non-parametric Mann-Whitney Wilcoxon (MWW) test. One-way ANOVA was also used to evaluate the statistical significance of the difference in response time to reach specific levels (10, 30%) of the peak percentage signal changes after multiple comparison corrections. To understand the lateralization of responses for both stimulus conditions, we assessed the p-value associated with the GLM analysis separately for each ROI in the left and right hemispheres, applying a t-threshold level of more than 2. Comparison of mean p-statistics between cortical areas present in either or both hemispheres aids in understanding the response lateralization, given that heat stimulation was administered to the left hand.

2.5. FUS parameters and presentation paradigm

A 128-element transducer array (radius of curvature = 72 mm, outer diameter = 103 mm, element diameter = 6.6 mm, free-field full-width half max 9.3 mm and 2.2 mm in the axial and lateral directions [30], manufactured by Imasonic (Besancon, France) was used in the current study and was placed around the midline of the head. The scalp was shaved, and a chemical depilatory cream was applied before transmission gel was placed on the scalp to ensure adequate acoustic coupling. The FUS stimulation blocks consisted of trains of 650 kHz pulses, 500 ms pulse train duration, pulse repetition frequency (PRF) of 1 kHz, and pulse duration of 0.5 ms. Detailed FUS parameters are reported in the Supplementary Table 1. This pulse train was repeated at 0.5 Hz for 16 s. Individual pulses were ramped up and down (ramp duration 50 us) to reduce spectral content in the auditory range [31]. Our target *in vivo* pressure was 550 kPa. This was estimated based on a transmission percentage of 39%. Steering compensation was performed based on hydrophone measurements of the beam during lateral steering of the transducer. A custom cone was filled with water (approximately 10% H_2O and 90% D_2O) and connected to a degassing circuit to minimize bubble formation in the fluid. D_2O was used to reduce geometric distortions of the MR images due to ineffective shimming of the water concentration in the cone. Water was recovered after every experiment, and the percentage changed due to dilution with regular water from the degassing circuit. The transducer was driven by a custom-built amplifier

system (Image Guided Therapy, Pessac, France) and controlled through a custom Python program.

2.6. Use of optical tracking and MRI-ARFI to localize ultrasound beam on target

Delivering FUS modulation at the intended target with high precision is critical for our studies. Prior to applying FUS modulation, we validated the location of the acoustic focus at the intended target, thalamic VPL nucleus, through a three-step procedure, which is illustrated in Fig. 1. First, we performed an fMRI mapping study to functionally localize the VPL nucleus target responsive to nociceptive heat stimulation in each animal. Fig. 1C shows one representative heat stimulation evoked fMRI activation map. Second, we used optical tracking to guide the placement of the FUS transducer so that the free-field focus would be located at the functionally pre-defined heat responsive nuclei (see the crosshairs shown in Fig. 1Da–c). Fig. 1B shows the schematics of the optical tracking system. Six MRI-visible fiducial markers with an outer diameter of 15 mm and an inner diameter of 4.5 mm (MM3002, IZI Medical Products, Owings Mills, MD) were placed on the stereotactic frame (one on each eye bar and two on the two ear bars) to enable optical tracking outside the MRI scanner. Briefly, a T1-weighted image was acquired to localize the fiducial markers placed around the transducer frame for guiding optical tracking of the FUS focus. The location and trajectory of the free-field FUS beam were estimated by tracking the position of the transducer (NDI Polaris, Ontario, Canada) and registering its position in physical space to the imaging space relative to the fixed positions of the fiducials. By determining the transducer location during optical tracking, the projected free-field focus and the subsequently acquired MR acoustic radiation force imaging (MR-ARFI) displacement image could be overlaid on MR images in the targeted brain region where BOLD activation foci were encoded (Fig. 1D). Detailed equations describing the coordinate transform relating these image volumes (optically tracked FUS beam, MR-ARFI displacement image, and anatomical scans) are provided in prior work [32].

MR-ARFI (Fig. 1D) measures the transient tissue displacements induced by a short FUS pulse [33–35]. If the ARFI displacement image of the FUS beam focus was not positioned at the right VPL contralateral to the left hand being stimulated, it was steered until the desired target was reached. Displacement images were acquired using a 3D spin-echo MRI acquisition (130 × 130 × 16 mm^3 FOV; acquisition 65 × 65 × 4 matrix; 2.0 × 2.0 × 4.0 mm^3 acquired voxel size; 112 × 112 × 4 reconstruction matrix; 1.16 × 1.16 × 4 mm^3 reconstructed voxel size; TE/TR 34/500 ms) with unipolar motion-encoding gradients (8 ms duration; 40 $mT•m^{-1}$ strength) to generate ARFI contrast. The motion-encoding gradients were oriented parallel to the ultrasound beam and the slices were positioned centered at the target with the slice direction corresponding to the long axis of the FUS beam (Fig. 1D). Sonications were performed at 650 kHz for 8.5 ms with a maximum *in vivo* pressure of 3.5 MPa and a duty cycle of 0.85%. Displacement images were reconstructed using complex phase subtraction of four phase images with switched polarity motion-encoding gradients and with or without sonications, which were acquired in an interleaved fashion, for a total scan time of 6.0 min to produce one displacement image. Images were reconstructed offline in MATLAB 2020a (MathWorks, Natick, MA). Our MR-ARFI beam mapping method was non-invasive and followed our and others' prior work [11,34,36,37].

2.7. Annotation of MR-ARFI target and cortical areas

We used a nonhuman primate (NHP) MRI atlas to annotate the thalamic nuclei targeted by the MR ARFI beam. The right, anterior, and superior coordinates associated with the centroid of MR-ARFI focus were used to construct a mask (with a diameter of 3 mm) in the native space of each subject. Both rigid and non-rigid transformation (warping), previously utilized to normalize the data into the template space, were applied to the mask. The transformed mask delineates the thalamic nuclei targeted. The specific thalamic nuclei being modulated are annotated by the macaque monkey atlas. Fig. 2A displays the registration steps from the native subject-level 3D T1 weighted images to the normalized map and then to the NHP template atlas. MR-ARFI images were thresholded to localize the FUS activation focus in each subject space. Fig. 2B shows examples from one NHP subject, where the thalamic nuclei that displayed heat-stimulus evoked activations were indicated by "*". The FUS beam interacted with seven thalamic nuclei in this case. The specific nuclei are listed at the bottom of Fig. 2. Across subjects, five thalamic nuclei were consistently stimulated, including centromedial_parafascicular (CM_Parafas) (2), mediodorsal (MD) (3), ventral_lateral (VL) (4), ventral_lateral_posteroventral (VLpv) (5), and ventroposterior_medial_and_lateral (VPm&VPl) (6).

3. Results

3.1. Effects of concurrent FUS stimulation of thalamic VPL nucleus on heat responses at the target and whole-brain off-target regions

Delivery of 47.5 °C heat stimuli on fingers elicited widespread BOLD fMRI activations. Fig. 3 shows the group-level activated brain regions under heat (A) or heat + FUS (B) stimulation conditions. Heat-evoked activations were detected in 24 regions, including areas involved in the processing of sensory aspects (VPL nucleus, the primary (SI) and secondary (SII) somatosensory areas, area 7, and floor of the lateral sulcus (FSL, containing insular cortex)), emotional and affective aspects (components of ACC, MCC, and PCC), and cognitive aspects (dorsolateral (dPFC) and ventrolateral (vlPFC) prefrontal areas) of nociceptive information (Fig. 3A and B). Interestingly, other sensory cortices, including visual (V2–V3) and auditory areas (BAAC and CAAC), as well as primary motor cortex (M1/PM), supplementary motor area (pre-SMA), and associative areas (ventromedial intraparietal, vmIPS) were also functionally active. Many of the heat nociceptive stimulus-responsive areas were among the most consistently activated brain regions in human pain fMRI studies [38]. From the whole brain network perspective, heat nociceptive stimulation engaged brain regions belong to visual (V2–V3), sensorimotor (SI, SII, area 7, FLS, M1/PM, and pre-SMA), dorsal attention (intraparietal sulcus), limbic (cingulate gyrus), and frontoparietal (FPN) networks. The Brodmann Area 8 is equivalent to the frontal eye field in the human brain, which is a part of the frontal cortex and the dorsal attention network [39–41]. Area 5 is part of the posterior parietal cortex and is involved in somatosensory processing, movement, and association [42]. The superior temporal area (MST) is engaged in auditory processing and has also been implicated as a critical structure in social cognition [43]. Similarly, TEO belongs to the inferior temporal cortex and is involved in visual pattern discrimination [44]. Color-coded ROI activation map is illustrated in Supplementary Fig. 1 (color sequence is in order with Table 1). Fig. 3C and D presents selected activation foci in

the SI, SII, Insular (FSL), ACC, and MCC cortex under heat stimulation, with activations in other areas masked out.

Responses in some regions were bilateral, while others were unilateral, being observed either in the contralateral (right) or ipsilateral (left) side of the hemisphere. Although heat stimuli were applied to the left hand, Table 1 summarizes the activated areas in both hemispheres. All primary somatosensory and motor regions, including thalamic VPL, SI, SII, insular, area 5, and M1/PM, along with ACC, showed bilateral stimulus activation. Cognitive areas in the ipsilateral hemisphere, such as DPC and vlPFC, responded to the heat stimulus. In contrast, the MCC, area 7 m, and TP in the contralateral hemisphere exhibited responses.

Fig. 3A and B shows that concurrent sonication of the VPL and surrounding nuclei during nociceptive heat stimulation altered the fMRI activation patterns at the whole brain heat nociceptive processing network level. The FUS parameters were selected because they have induced suppressive effects on the tactile stimulation-evoked BOLD fMRI activations [11,14,34]. When FUS stimulation was concurrently delivered, the number of detected activations reduced from 24 to 19 cortical areas, respectively. Out of the 24 areas responsive to heat, nine (indicated by “n” in the table) lost detectable activation under heat + FUS condition, demonstrating the suppressive effect of FUS modulation. Interestingly, four areas that did not show activation during heat stimulation did exhibit detectable responses during the heat + FUS condition. Table 1 outlined FUS-affected, heat-responsive regions into three categories: jointly activated (indicated by blue font), suppressed (black font), and enhanced (red font). The nine cortical areas lost detectable BOLD signal change are MCC, area 8A, vlPFC, preSMA, SII, vmIPS, area 7 m, TP, and TEO, all of which These areas associated with sensory, multisensory, and sensorimotor integration. The four areas that exhibited strong responses under heat + FUS conditions were caudal orbital frontal cortex (COFC), lateral intraparietal sulcus (IIPS), caudal superior temporal gyrus (STGc), and middle temporal area (MT).

A close examination of the activation in both hemispheres, focused on selected foci in the SI, SII, Insular (FSL), ACC, and MCC cortex (shown in Fig. 3C), revealed significant suppression of the heat response. This suppression, indicated by the loss of activation, was observed in the contralateral ACC and FSL, ipsilateral SI, and in bilateral SII and MCC. This differential suppression on contra-versus ipsilateral hemispheric regions is particularly intriguing given the left VPL heat response was suppressed (as seen in Fig. 5).

We also assessed the hemispheric dominance of fMRI activations induced by heat or heat + FUS. Statistical analysis results (p-values) are presented in the middle and right columns for heat or heat + FUS conditions in Table 1. As the mean p value (post FDR correction) is evaluated for ROIs that meet the t-value threshold (>2), a smaller p-value indicates stronger activation in the ROI. Hence, a direct comparison of p-values can reveal response asymmetry between ipsilateral and contralateral cortical areas. When the animals’ left hand was stimulated, 15 out of 24 heat-responsive cortical areas showed activations on one hemisphere (see the middle column in Table 1). Some areas on the contralateral side (right hemisphere, including MCC, Area 7 m and TP) had stronger activations, while others on

the ipsilateral side (left hemisphere, such as Area 8A, DPC, vlPFC, LMC, vmIPS, MST and Area 7 to stimulus) showed a stronger response. These inter-hemispheric differences suggest some degree of hemisphere dominance is present during the processing of unilateral nociceptive inputs. Bilateral activation was detected in ACC, preSMA, SI, SII, Area 5, VPL, PCgG, STGr, and insula (FLS). When suppressive FUS was delivered to the right thalamic nuclei, inter-hemisphere differences with stronger cortical responses in the contralateral right hemisphere were observed in DPC, LMC, SI, MST, Area 7, cACC and V2–V3, compared to the heat stimulus condition (compare the right with the middle columns in Table 1). Hemispheric shifts during FUS modulation were noted in DPC (L4 versus R4) and visual cortex (L24 versus R24).

Fig. 4 shows the heat versus heat + FUS subtraction maps. The thalamic VPL nuclei along with fifteen cortical areas, including ACC, MCCm vlPFC, PCgG, SII, area 7, area 7 m, preSMA, V2–V3, LMC, TEO, STSf, and STGr/STSd, exhibited most significant heat evoked signal changes when thalamic heat response was suppressed by FUS. These affected cortical regions belong to different pain networks and are responsible for multidimensional pain processing in primates [45,46]. The results demonstrated that a reduction in VPL nociceptive responses leads to widespread disruption of the network functions.

3.2. Effects of concurrent FUS on heat evoked BOLD signal amplitudes at thalamus and off-target cortical areas

The time courses of percentage BOLD signal changes (PSC), averaged over the stimulus cycle in selected brain regions, confirmed the fMRI activation detected during heat versus heat + FUS stimulation conditions (as depicted in Fig. 3). In the FUS-targeted VPL nucleus, the heat-evoked BOLD signal change was significantly weaker when FUS was delivered concurrently (refer to the blue and red curves comparison in Fig. 5A). Similar signal reductions were evident in most off-target areas, including SI, ACC, M1/PM, area 7, FLS, DPC, SII, MCC, and preSMA. In areas displaying bilateral activation, no significant differences were found between the left and right hemispheres. Representative time courses from ROIs in both hemispheres are illustrated in Supplementary Fig. 2. Fig. 5B shows the difference in peak BOLD signal changes (mean ± standard error) between the heat and heat + FUS conditions for each area, irrespective of its hemisphere dominance. The peak signal reductions caused by FUS are approximately 67% at the VPL target (heat/(heat + FUS): 0.43/0.14 ± 0.02/0.02), 80% in area vlPFCs (0.50/0.10 ± 0.02/0.02), 71% in ACC (0.60/0.16 ± 0.02/0.02), and 77% in DPC (0.50/0.11 ± 0.01/0.01), as detailed in Fig. 5C. Fig. 5C further elucidates the signal reductions resulting from FUS thalamic suppression at each ROI, considering the heat + FUS response as the baseline. In two of the four brain regions (COFC and MT), the PSC changes were both reversed and more pronounced in the heat + FUS condition compared to the heat-only conditions. The statistical significance was quantified using pairwise MWW (Mann Whitney Wilcoxon) tests with “*/**” indicating p-values < 0.05 and 0.005, respectively.

3.3. FUS suppression of thalamic heat response altered the flow of information

We quantified the latencies of the early phase BOLD signal increases to reach 10%, and 30% of the peak in each ROI and plotted these latencies in ascending order for both

heat and heat + FUS conditions. Fig. 6A and B shows the whisker boxplots of the group-level variation of the response time needed to reach 10% and 30% of the peak PSC under both experimental conditions. The correlation between the response latencies and the ROI order is strong (r-value: correlation coefficient) and statistically significant (p-value). However, the sequence of information processing flow differed markedly between the two conditions (compare boxplots with red/blue boundaries: heat/heat + FUS). During natural heat stimulation, VPL nucleus is the first supraspinal relay station for processing nociceptive heat inputs originating from the hand, with DPC (dorsal frontal cortex) being the last region within the network. The information processing sequence was as follows: VPL-FLS-MCC-SII-vlPFC-SI-ACC-area 7-M1/PM-DPC. The linear trends are statistically significant at 10% ($r = 0.97$, $p < 0.0005$) and 30% ($r = 0.95$, $p < 0.0005$). To further illustrate the impact of FUS on the order of information flow, we presented the latencies in the heat + FUS condition in order, as observed in the heat stimulation condition. The disruption in the latency order is evident, as indicated by low correlation r and p values (blue dotted line). A high p-value associated with poor correlation suggests not only that FUS suppresses the response, but the degree of alteration in response latency also varies across specific ROIs.

Fig. 6C displays the two gamma-fitted curves of block-averaged percentage signal change at each representative ROI. The estimated BOLD time course illustrates the variation in time to reach 10, and 30% of the peak value time points during heat stimulation. Fig. 6D and E shows that the response latency differences between most ROI pairs significantly changed when comparing heat and heat + FUS conditions (e.g., ANOVA, $p < 0.05$ between SII and VPL and $p < 0.005$ between SII and VPL in heat only condition in Fig. 6D). The asterisk in Fig. 6E refers to the ROI pairs that lost their response latency differences when the VPL and surrounding nuclei were suppressed (under heat + FUS condition).

3.4. Schematic summary of the reorganization of brain-wise heat nociceptive networks after thalamic VPL suppression

Fig. 7 visualizes the sequence of information processing within nine selected cortical areas and the VPL nucleus. The suppression of heat nociceptive responses at the thalamic VPL nucleus significantly impacted the entire brain's nociceptive responses. This suppression affected regions that belong to multiple well-established nociceptive and associated networks, leading to a substantial reorganization of the information processing flow and pathways. The impacted networks include visual (V2 and V3), sensorimotor (SI, SII, M1/PM, preSMA), dorsal attention (ventromedial intraparietal sulcus, vmIPS), limbic (ACC and MCC), and default mode (middle temporal cortex, medial superior temporal area) networks.

Higher-order sensory areas affected encompass Area 5, Area 7, Area 7 m, the auditory cortex (BAAC and CAAC), and the floor of the lateral sulcus (including VS subregion of SII, posterior insula, and para-insula). Other regions include Area 8A, dlPFC, vlPFC, TG temporal pole, TEO area, the fundus of the superior temporal sulcus, the rostral superior temporal region, caudal superior temporal gyrus, middle temporal area, lateral intraparietal sulcus, and caudal orbital frontal cortex. The suppression of the thalamic nociceptive response drastically altered the nociceptive information processing flow and pathways.

4. Discussion

In this study, we demonstrated the effectiveness of transcranial FUS in targeting and suppressing nociceptive heat-evoked BOLD responses in deep brain regions, particularly a group of thalamic nuclei surrounding VPL. This resulted in a diminished nociceptive response across cortical areas encompassing both sensory and non-sensory nociceptive networks, along with non-nociceptive networks. By directly eliminating thalamic heat nociceptive responses, we triggered a complete reorganization of thalamocortical networks and consequently altered the pathways and direction of nociceptive information processing. The suppressive effects induced by low-intensity FUS align with our previous observations in the NHP primary somatosensory cortex and network [13,14]. Although the study was conducted on anesthetized monkeys without behavior assessment, the robustness of FUS modulation and the notable disruption of the nociception network could hold significant implications for future clinical applications. The concept and method are easily translatable. We wish to clarify that ‘pain’ is a term specifically used to describe conscious pain perception, which can only be evaluated in human subjects. Throughout the discussion, we intended was to use the terms ‘nociception’ and ‘nociceptive network or matrix’ to characterize our observations derived from anesthetized animal subjects. Nociceptive regions and networks are preserved and can be investigated in anesthetized animals.

4.1. The involvement of thalamic nuclei in thermal pain

Both human and NHP fMRI studies have identified the involvement of multiple thalamic nuclei in pain perception [47] and nociceptive processing [18]. The current hypothesis posits that different nuclei serve as functionally distinct relay and integration stations for processing information associated with multidimensional pain experiences. Historically, the ventral caudal (VC) nucleus in humans has been targeted for Deep Brain Stimulation (DBS) for chronic pain relief. Yet, its therapeutic benefits and underlying mechanisms of action remain largely unestablished [24,48], leading to a decline in the number of procedures performed. Other thalamic targets have been explored; a recent FUS study has demonstrated that FUS stimulation of the anterior thalamus changed pain thresholds in healthy subjects [9]. Alternatively, cingulotomy is performed for pain relief in late-stage cancer pain patients. The anterior cingulate cortex (ACC) receives direct thalamic input from the thalamic mediodorsal (MD) nucleus, as demonstrated by an anatomical tracing study in NHP [49]. In our study, thermal heat-evoked activation was detected in the contralateral MD nucleus relative to the stimulated hand, supporting its involvement in thermal nociceptive processing.

To further explore the role of thalamic nuclei and their thalamocortical network in thermal nociception processing, we employed a unique approach in this MRgFUS neuromodulation study using NHPs. To ensure accurate modulation of thalamic activity, we first mapped the nociceptive region in each subject by stimulating one hand with nociceptive heat stimuli, using their responses as a functional localizer to identify FUS targets. We then confirmed the intended FUS target location using MR-ARFI images. Employing FUS parameters proven to induce suppressive neuromodulation in the somatosensory cortex [13], we demonstrated that MRgFUS can robustly and noninvasively suppress nociceptive signals in deep brain regions. In this study, we provided functional evidence suggesting that a reduction in thalamic heat

nociceptive response can lead to widespread reduction in numerous cortical areas within and beyond the nociceptive information processing network.

In accordance with our findings, recent studies have provided growing evidence that FUS can indeed modulate human brain functions (for a recent review, see Ref. [50]), including pain perceptions [9]. Yet, the brain circuit mechanisms mediating the changes in pain perception threshold through FUS targeting the anterior thalamus remain to be fully elucidated. We acknowledge the appeal of a therapeutic tool that delivers sustained effects post-FUS modulation. The question of whether FUS induce such long-lasting effects is currently an open area of inquiry. Prior research has highlighted that FUS can influence behavior and alter resting state functional networks in human subjects as reviewed by Ref. [50]. In line with this, our ongoing study and unpublished findings suggest that FUS exposure significantly reshapes the nociceptive processing network. We therefore propose that FUS could serve as an acute assessment tool, enabling the identification of individual patient-specific brain targets and assisting in the selection of patients mostly to benefit from ablation or DBS procedures.

Future studies involving awake human subjects or chronic pain patients are needed to establish the link between reductions in pain-related BOLD signals in many brain regions to a decrease in pain sensation [51, 52]. Our findings support the translation of FUS parameters and targets for future clinical applications in chronic pain patients. Notably, to our knowledge, this is the first study that directly probes the causal relationships between the nociceptive processing in thalamic nuclei and the rest of the brain in primates. FUS suppression of the nuclei in the thalamus has the potential to serve as a pain relief therapy. Several groups, including our own, are actively pursuing future clinical trials to address these critical questions.

4.2. Off-target effects of FUS suppression of thalamic activity

Two types of reactions were observed in the cortex when thalamic heat nociceptive responses were suppressed by FUS. Most cortical areas, both within and beyond the established nociceptive networks (see Fig. 7), exhibited reductions in BOLD signal amplitude in response to nociceptive heat stimuli. These reductions could be direct consequences of the thalamic response reduction via causal connections to the central posterolateral (VPL) nucleus of the thalamus, which was the main focus of this study. Interestingly, four cortical areas that did not previously respond to painful stimuli began to display a strong painful heat response when the thalamus response was suppressed. This observation could be explained by the unmasking or relief of tonic suppression from the thalamus, suggesting that removal of thalamic suppression likely led to rebounds in their responses to nociceptive stimuli. These four areas belong to higher-order cognitive control and attention networks, which likely provide top-down control of thalamic pain processing [53]. This observation provides the first line of evidence supporting the top-down causal connections from higher-order brain regions to thalamic sensory nucleus. It’s important to note that nociceptive heat-evoked responses in these cortical areas were observed in anesthetized NHPs. As demonstrated in our past research, many higher-order brain regions,

such as the prefrontal cortex, are involved in nociceptive information processing even without consciousness. Their roles in pain perception remain to be established.

Our study emphasizes the brain-wide engagement in nociceptive processing and the pivotal role of the thalamic nuclei. A set of fine-scale cortical areas of particular note are those identified along the lateral sulcus. In addition to the well-documented secondary somatosensory cortex (SII) and posterior insular cortex, area 7 and retro-insula (annotated as FLS by the atlas in this study) consistently responded to heat nociceptive stimulation in both the current and our previous high-resolution NHP studies at 9.4T [45,54–58]. Latency analysis revealed that FLS and SII cortex responded as early as, or earlier than, the SI cortex. This observation supports the hypothesis that lateral sulcus areas are the "primary" nociceptive-specific cortical processing areas [59,60]. Focal lesions of this region have led to altered "pain sensation" in humans [61]. These areas not only exhibited robust nociceptive heat responses but were also causally modulated by changes in nociception-associated activity in the thalamic sensory and surrounding nuclei. The modulations are more widespread and complex than anticipated.

Another interesting finding is that the unilateral suppression of the right thalamic heat response resulted in distinct modulation of cortical areas on different hemispheres, as shown in Fig. 3C and Table 1. For example, the suppression of right thalamic heat response, evoked by left-hand stimulation, led to response reductions in ipsilateral S1 and contralateral insula (FSL) and ACC. This observation suggests functional connections between somatosensory and higher-order areas exhibit hemispheric differences. SI, DPC, and VPL within the same hemisphere are more tightly interconnected. The insula and ACC on the opposite hemisphere have strong interconnections with the VPL. The VPL's connection to S2, MCC, and vlPFC appear to be comparable, as suppression of VPL resulted in response reductions in bilateral regions. These observations have important clinical implications since many chronic pain conditions are lateralized on one side of the body.

We detected nociceptive heat responses in at least one cortical area within each functional network, including visual, somatomotor, auditory, dorsal, ventral attention, limbic, fronto-parietal, and default mode networks [38]. Interestingly, nociceptive heat-evoked BOLD signal changes were detected in cortical areas not previously associated with established human pain and associative networks. Heat responses were also observed in temporal, parietal, prefrontal and frontal areas. Most importantly, these cortical areas have direct functional connections to the thalamus sensory nucleus. The functional relationships of these thalamocortical connections during nociceptive processing warrant further investigation.

4.3. The value of fMRI monitoring and disruption of nociceptive thalamocortical network

Suppression of nociceptive responses in VPL and surrounding thalamic nuclei completely disrupted the normal information processing flow and reorganized the pathways, as illustrated in Fig. 7. The general ascending processing flow from somatosensory to higher-order associative sensory, affective, and cognitive regions is evident under normal nociceptive processing conditions. Within the somatosensory system, processing in SII and FLS occurs early along the pathway. This finding is consistent with our previous NHP studies, wherein subsequent intracortical electrophysiology recordings studies validated the

neuronal basis of nociceptive heat-evoked fMRI signals [62]. These previous studies indicate that heat nociceptive stimulus-evoked fMRI signals are reliable indicators of nociceptive neuron activity. In the current study, one of the novel findings is that FUS suppression of thalamus response reversed the direction of the information processing flow. Nociceptive signals reached the dorsal prefrontal (DFC) cortex first and then flowed down to sensory cortices. Existing studies support the notion that increases in early-phase BOLD signals correlates strongly with increases in neural activity [63]. This previous study forms the foundation for our current approach. Here, we adopted the latency of signal increase for quantifying the inter-area information flow.

4.4. Implications for FUS-induced fMRI signal changes detected in off-target higher-order brain regions

Higher-order cortical areas, including the SII, posterior insula, MCC, and ACC, are involved in multiple brain functions and are not exclusively engaged in nociception [64,65]. Therefore, changes in fMRI signals could signify a variety of distinct neural processes. Our study was not designed to explore these aspects; we only compared heat versus heat + FUS stimulation conditions. We acknowledge the uncertainty surrounding the existence of nociceptive processes in higher-order brain regions, such as the PFC, and the reasons why temporo-occipital areas are activated during the processing of nociceptive heat inputs. The activation in the visual cortex might represent spurious activation due to factors unrelated to pain. Indeed, activation of temporo-occipital areas has been revealed by several neuroimaging studies during REM-sleep [66]. We intended to draw parallels between brain regions within the ‘pain matrix’ in humans and those found in the ‘nociception matrix’ in anesthetized animals. As highlighted by Apkarian et al. in their 2005 review [67], a substantial knowledge gap between fMRI studies of pain in healthy individuals and those with diseases, especially concerning the underlying neural electrophysiology. This gap hinders our comprehensive understanding of the roles of these regions. Further investigations from an electrophysiological perspective in both humans and animals are required to fully comprehend the contributions of these higher-order areas to nociception and pain perception.

4.5. Challenges in targeting deep brain structure and the value of real-time ARFI feedback

The results of our study underscore the importance of real-time feedback for delivering FUS modulation with utmost accuracy and precision. In our research, we used a 128-element ultrasound array because it offers focal stimulation at a millimeter scale. Despite its small focus, it interacted with five thalamic nuclei, some of which are involved in processing nociceptive stimuli. In this context, the off-target effects resulted from the suppression of a group of thalamic nuclei. For upcoming clinical applications, real-time feedback via MR-ARFI will be vital for optimizing targets. The beam-steering capacity of the FUS system could, in principle, also assist in refining the FUS target for chronic pain relief. Leveraging this capability, it might be feasible to assess the perceptual outcomes of FUS stimulation on individual thalamic nuclei or a collective group.

4.6. Limitations of the study

The primary limitation of this study is the use of anesthesia. Isoflurane anesthesia is known to suppress neural activity and reduce the BOLD signal fluctuation in high-frequency bands [68,69]. Interestingly, our study found that many brain regions associated with pain perception in awake humans were also activated under anesthesia. This suggests that numerous higher-order cortical areas are engaged in nociceptive processing even in the absence of conciseness. Another associated limitation is the lack of pain behavior assessment. Quantifying pain-related behavior in NHPs is challenging due to practical and ethical considerations. To date, our MRI safety investigations in these monkeys have not detected any tissue damage caused by ultrasound exposure. The safety record of our MRgFUS system and protocol presents an optimistic prospect for the subsequent phase of translational studies in human subjects.

We emphasize the need for caution when comparing and interpreting fMRI findings from ‘pain’ conditions in human subjects with those observed in ‘nociceptive’ conditions in anesthetized animals. For instance, a robust LFP study underscores the significance of prefrontal and parietal areas in the conscious perception of pain [70]. Future research is essential to fully comprehend how the activity in high-order cortical areas, such as the prefrontal cortex and ACC, contributes to the conscious perception of pain – a task replete with challenges [70,71].

It’s pertinent to note that while conscious pain perception emerges from the collective processes and integration of painful information across numerous spinal and brain regions along the neural axis, these fundamental processes remain intact and are investigable in anesthetized animals. For example, we have previously demonstrated a close association between the activity of nociceptive neurons and fMRI signal changes evoked by identical nociceptive stimuli in somatosensory cortices [72]. Moreover, our research, complemented by others, has indicated that heat stimulation of 47.5 °C activates nociceptive neurons and can evoke a sensation of burning pain in human subjects. FMRI signals can distinguish brain responses to nociceptive versus innocuous stimuli [72]. Many brain regions that exhibited fMRI responses to nociceptive stimuli in our study also displayed fMRI signal changes in human subjects during pain perception. Such a correlation bolsters the functional relevance of fMRI responses to nociceptive stimuli, even in anesthetized animals.

4.7. In summary

We have demonstrated that transcranial focused ultrasound is a potent neuromodulation tool with significant potential for manipulating brain networks and possibly for future pain management. Manipulating nociceptive processing circuits by inhibiting thalamic nuclei resulted in brain-wide changes in nociceptive responses and associated processing pathways. These thalamic nuclei emerge as potential targets for neuromodulation aimed at pain relief. Adapting the MRgFUS system for clinical use will also improve our mechanistic understanding of the analgesic effects of thalamic nucleus stimulation. NHPs provide an ideal model for developing FUS neuromodulation protocols.

Supplementary Material

Refer to Web version on PubMed Central for supplementary material.

Acknowledgements

We want to thank Chaohui Tang for her assistance in data collection and animal care.

Funding sources

This work was funded by National Institutes of Health grants U18 EB029351, R01MH111877, 1S10OD012297-01A1, and 5T32EB014841.

Data availability statement

The data, documentation and code that support the findings of this study will be made available in the publicly available repository: http://openneuro.org.

Abbreviations

FUS	transcranial focused ultrasound
fMRI	functional magnetic resonance imaging
BOLD	blood-oxygen-level-dependent imaging
MR-ARFI	magnetic resonance-acoustic radiation force imaging
HRF	hemodynamic response function; ROI, regions of interest

References

[1]. Wang P, et al. Brain modulatory effects by low-intensity transcranial ultrasound stimulation (TUS): a systematic review on both animal and human studies. Front Neurosci 2019;13:696. [PubMed: 31396029]

[2]. Beric A. Transcranial electrical and magnetic stimulation. Adv Neurol 1993;63: 29–42. [PubMed: 8279314]

[3]. Turi Z, Paulus W, Antal A. Functional neuroimaging and transcranial electrical stimulation. Clin EEG Neurosci 2012;43(3):200–8. [PubMed: 22956648]

[4]. Saiote C, et al. Combining functional magnetic resonance imaging with transcranial electrical stimulation. Front Hum Neurosci 2013;7:435. [PubMed: 23935578]

[5]. Nahas Z, et al. Unilateral left prefrontal transcranial magnetic stimulation (TMS) produces intensity-dependent bilateral effects as measured by interleaved BOLD fMRI. Biol Psychiatr 2001;50(9):712–20.

[6]. Haraldsson HM, et al. Transcranial Magnetic Stimulation in the investigation and treatment of schizophrenia: a review. Schizophr Res 2004;71(1):1–16. [PubMed: 15374567]

[7]. Pollak TA, et al. A systematic review of transcranial magnetic stimulation in the treatment of functional (conversion) neurological symptoms. J Neurol Neurosurg Psychiatry 2014;85(2):191–7. [PubMed: 23303960]

[8]. Badran BW, et al. Sonication of the anterior thalamus with MRI-guided transcranial focused ultrasound (tFUS) alters pain thresholds in healthy adults: a double-blind, sham-controlled study. Focus 2022;20(1):90–9. [PubMed: 35746940]

[9]. Badran BW, et al. Sonication of the anterior thalamus with MRI-Guided transcranial focused ultrasound (tFUS) alters pain thresholds in healthy adults: a double-blind, sham-controlled study. Brain Stimul 2020;13(6):1805–12. [PubMed: 33127579]

[10]. Darmani G, et al. Non-invasive transcranial ultrasound stimulation for neuromodulation. Clin Neurophysiol 2022;135:51–73. [PubMed: 35033772]

[11]. Legon W, et al. Transcranial focused ultrasound neuromodulation of the human primary motor cortex. Sci Rep 2018;8(1):10007.

[12]. Yang PF, et al. Differential dose responses of transcranial focused ultrasound at brain regions indicate causal interactions. Brain Stimul 2022;15(6):1552–64. [PubMed: 36496128]

[13]. Yang PF, et al. Bidirectional and state-dependent modulation of brain activity by transcranial focused ultrasound in non-human primates. Brain Stimul 2021;14(2): 261–72. [PubMed: 33460838]

[14]. Yang PF, et al. Neuromodulation of sensory networks in monkey brain by focused ultrasound with MRI guidance and detection. Sci Rep 2018;8(1):7993. [PubMed: 29789605]

[15]. Naor O, Krupa S, Shoham S. Ultrasonic neuromodulation. J Neural Eng 2016;13(3): 031003.

[16]. Legon W, et al. Transcranial focused ultrasound modulates the activity of primary somatosensory cortex in humans. Nat Neurosci 2014;17(2):322–9. [PubMed: 24413698]

[17]. Silvanto J, et al. Neural adaptation reveals state-dependent effects of transcranial magnetic stimulation. Eur J Neurosci 2007;25(6):1874–81. [PubMed: 17408427]

[18]. Willis WD, Westlund KN. Neuroanatomy of the pain system and of the pathways that modulate pain. J Clin Neurophysiol 1997;14(1):2–31. [PubMed: 9013357]

[19]. Youssef AM, et al. Shifting brain circuits in pain chronicity. Hum Brain Mapp 2019; 40(15):4381–96. [PubMed: 31298464]

[20]. Wu R, et al. Graph theory analysis identified two hubs that connect sensorimotor and cognitive and cortical and subcortical nociceptive networks in the non-human primate. Neuroimage 2022;257:119244.

[21]. Davis KD, et al. Thalamic stimulation-evoked sensations in chronic pain patients and in nonpain (movement disorder) patients. J Neurophysiol 1996;75(3): 1026–37. [PubMed: 8867115]

[22]. Davis KD, et al. Phantom sensations generated by thalamic microstimulation. Nature 1998;391(6665):385–7. [PubMed: 9450753]

[23]. Carrera E, Bogousslavsky J. The thalamus and behavior: effects of anatomically distinct strokes. Neurology 2006;66(12):1817–23. [PubMed: 16801643]

[24]. Alamri A, Pereira EAC. Deep brain stimulation for chronic pain. Neurosurg Clin 2022;33(3):311–21.

[25]. Elias GJB, et al. Deep brain stimulation of the brainstem. Brain 2021;144(3): 712–23. [PubMed: 33313788]

[26]. Singleton WGB, Ashida R, Patel NK. Deep brain stimulation for facial pain. Prog Neurol Surg 2020;35:141–61. [PubMed: 32906139]

[27]. Plaksin M, Kimmel E, Shoham S. Cell-type-Selective effects of intramembrane cavitation as a unifying theoretical framework for ultrasonic neuromodulation. eNeuro 2016;3(3).

[28]. Seidlitz J, et al. A population MRI brain template and analysis tools for the macaque. Neuroimage 2018;170:121–31. [PubMed: 28461058]

[29]. Jung B, et al. A comprehensive macaque fMRI pipeline and hierarchical atlas. Neuroimage 2021;235:117997.

[30]. Chaplin V, Phipps MA, Caskey CF. A random phased-array for MR-guided transcranial ultrasound neuromodulation in non-human primates. Phys Med Biol 2018;63(10):105016.

[31]. Mohammadjavadi M, et al. Elimination of peripheral auditory pathway activation does not affect motor responses from ultrasound neuromodulation. Brain Stimul 2019;12(4):901–10. [PubMed: 30880027]

[32]. Phipps MA, et al. Considerations for ultrasound exposure during transcranial MR acoustic radiation force imaging. Sci Rep 2019;9(1):16235.

[33]. McDannold N, Maier SE. Magnetic resonance acoustic radiation force imaging. Med Phys 2008;35(8):3748–58. [PubMed: 18777934]

[34]. Ai L, et al. Effects of transcranial focused ultrasound on human primary motor cortex using 7T fMRI: a pilot study. BMC Neurosci 2018;19(1):56. [PubMed: 30217150]

[35]. Sarvazyan AP, et al. Shear wave elasticity imaging: a new ultrasonic technology of medical diagnostics. Ultrasound Med Biol 1998;24(9):1419–35. [PubMed: 10385964]

[36]. Gaur P, et al. Histologic safety of transcranial focused ultrasound neuromodulation and magnetic resonance acoustic radiation force imaging in rhesus macaques and sheep. Brain Stimul 2020;13(3):804–14. [PubMed: 32289711]

[37]. Ozenne V, et al. MRI monitoring of temperature and displacement for transcranial focus ultrasound applications. Neuroimage 2020;204:116236.

[38]. Lee JJ, et al. A neuroimaging biomarker for sustained experimental and clinical pain. Nat Med 2021;27(1):174–82. [PubMed: 33398159]

[39]. Reser DH, et al. Contrasting patterns of cortical input to architectural subdivisions of the area 8 complex: a retrograde tracing study in marmoset monkeys. Cerebr Cortex 2013;23(8):1901–22.

[40]. Paus T. Location and function of the human frontal eye-field: a selective review. Neuropsychologia 1996;34(6):475–83. [PubMed: 8736560]

[41]. Borra E, Luppino G. Comparative anatomy of the macaque and the human frontal oculomotor domain. Neurosci Biobehav Rev 2021;126:43–56. [PubMed: 33737106]

[42]. Ferrari-Toniolo S, et al. Posterior parietal cortex encoding of dynamic hand force underlying hand-object interaction. J Neurosci 2015;35(31):10899–910.

[43]. Kambeitz-Ilankovic L, et al. Modeling social sensory processing during social computerized cognitive training for psychosis spectrum: the resting-state approach. Front Psychiatry 2020;11:554475.

[44]. Distler C, et al. Cortical connections of inferior temporal area TEO in macaque monkeys. J Comp Neurol 1993;334(1):125–50. [PubMed: 8408755]

[45]. Chen LM. Cortical representation of pain and touch: evidence from combined functional neuroimaging and electrophysiology in non-human primates. Neurosci Bull 2018;34(1):165–77. [PubMed: 28466257]

[46]. Zhang X, et al. A multisensory fMRI investigation of nociceptive-preferential cortical regions and responses. Front Neurosci 2021;15:635733.

[47]. Yen CT, Lu PL. Thalamus and pain. Acta Anaesthesiol Taiwanica 2013;51(2): 73–80.

[48]. Leplus A, et al. Treatment of chronic refractory pain by combined deep brain stimulation of the anterior cingulum and sensory thalamus (EMOPAIN study): rationale and protocol of a feasibility and safety study. Brain Sci 2022;12(9).

[49]. Dum RP, Levinthal DJ, Strick PL. The spinothalamic system targets motor and sensory areas in the cerebral cortex of monkeys. J Neurosci 2009;29(45): 14223–35.

[50]. Sarica C, et al. Human Studies of Transcranial Ultrasound neuromodulation: a systematic review of effectiveness and safety. Brain Stimul 2022;15(3):737–46. [PubMed: 35533835]

[51]. Zhang M, et al. Thalamocortical mechanisms for nostalgia-induced analgesia. J Neurosci 2022;42(14):2963–72. [PubMed: 35232762]

[52]. Price DD, et al. Placebo analgesia is accompanied by large reductions in pain-related brain activity in irritable bowel syndrome patients. Pain 2007;127(1–2): 63–72. [PubMed: 16963184]

[53]. Ong WY, Stohler CS, Herr DR. Role of the prefrontal cortex in pain processing. Mol Neurobiol 2019;56(2):1137–66. [PubMed: 29876878]

[54]. Chen LM, et al. Biophysical and neural basis of resting state functional connectivity: evidence from non-human primates. Magn Reson Imaging 2017;39: 71–81. [PubMed: 28161319]

[55]. Wu R, et al. High-resolution functional MRI identified distinct global intrinsic functional networks of nociceptive posterior insula and S2 regions in squirrel monkey brain. Neuroimage 2017;155:147–58. [PubMed: 28461059]

[56]. Wu R, Yang PF, Chen LM. Correlated disruption of resting-state fMRI, LFP, and spike connectivity between area 3b and S2 following spinal cord injury in monkeys. J Neurosci 2017;37(46):11192–203.

[57]. Wang Z, et al. The relationship of anatomical and functional connectivity to resting-state connectivity in primate somatosensory cortex. Neuron 2013;78(6): 1116–26. [PubMed: 23791200]

[58]. Chen LM, et al. High-resolution maps of real and illusory tactile activation in primary somatosensory cortex in individual monkeys with functional magnetic resonance imaging and optical imaging. J Neurosci 2007;27(34):9181–91. [PubMed: 17715354]

[59]. Treede RD, et al. Cortical representation of pain: functional characterization of nociceptive areas near the lateral sulcus. Pain 2000;87(2):113–9. [PubMed: 10924804]

[60]. Craig AD, et al. Thermosensory activation of insular cortex. Nat Neurosci 2000;3 (2):184–90. [PubMed: 10649575]

[61]. Veldhuijzen DS, et al. Altered pain and thermal sensation in subjects with isolated parietal and insular cortical lesions. Eur J Pain 2010;14(5):535 e1–e11.

[62]. Ye X, et al. A thermal nociceptive patch in the S2 cortex of nonhuman primates: a combined functional magnetic resonance imaging and electrophysiology study. Pain 2021;162(11):2705–16. [PubMed: 33945242]

[63]. Jung WB, et al. Early fMRI responses to somatosensory and optogenetic stimulation reflect neural information flow. Proc Natl Acad Sci U S A 2021;118(11).

[64]. Iannetti GD, Mouraux A. Can the functional MRI responses to physical pain really tell us why social rejection “hurts”? Proc Natl Acad Sci U S A 2011;108(30):E343. author reply E344. [PubMed: 21712443]

[65]. Iannetti GD, Mouraux A. From the neuromatrix to the pain matrix (and back). Exp Brain Res 2010;205(1):1–12. [PubMed: 20607220]

[66]. Dang-Vu TT, et al. Functional neuroimaging insights into the physiology of human sleep. Sleep 2010;33(12):1589–603. [PubMed: 21120121]

[67]. Apkarian AV, et al. Human brain mechanisms of pain perception and regulation in health and disease. Eur J Pain 2005;9(4):463–84. [PubMed: 15979027]

[68]. Wu TL, et al. Effects of isoflurane anesthesia on resting-state fMRI signals and functional connectivity within primary somatosensory cortex of monkeys. Brain Behav 2016;6(12):e00591.

[69]. Hori Y, et al. Altered resting-state functional connectivity between awake and isoflurane anesthetized marmosets. Cerebr Cortex 2020;30(11):5943–59.

[70]. Bastuji H, et al. Convergence of sensory and limbic noxious input into the anterior insula and the emergence of pain from nociception. Sci Rep 2018;8(1):13360.

[71]. Bastuji H, et al. Pain networks from the inside: spatiotemporal analysis of brain responses leading from nociception to conscious perception. Hum Brain Mapp 2016;37(12):4301–15. [PubMed: 27391083]

[72]. Chen LM, et al. Differential fMRI activation to noxious heat and tactile stimuli in parasylvian areas of new world monkeys. Pain 2012;153(1):158–69. [PubMed: 22115923]

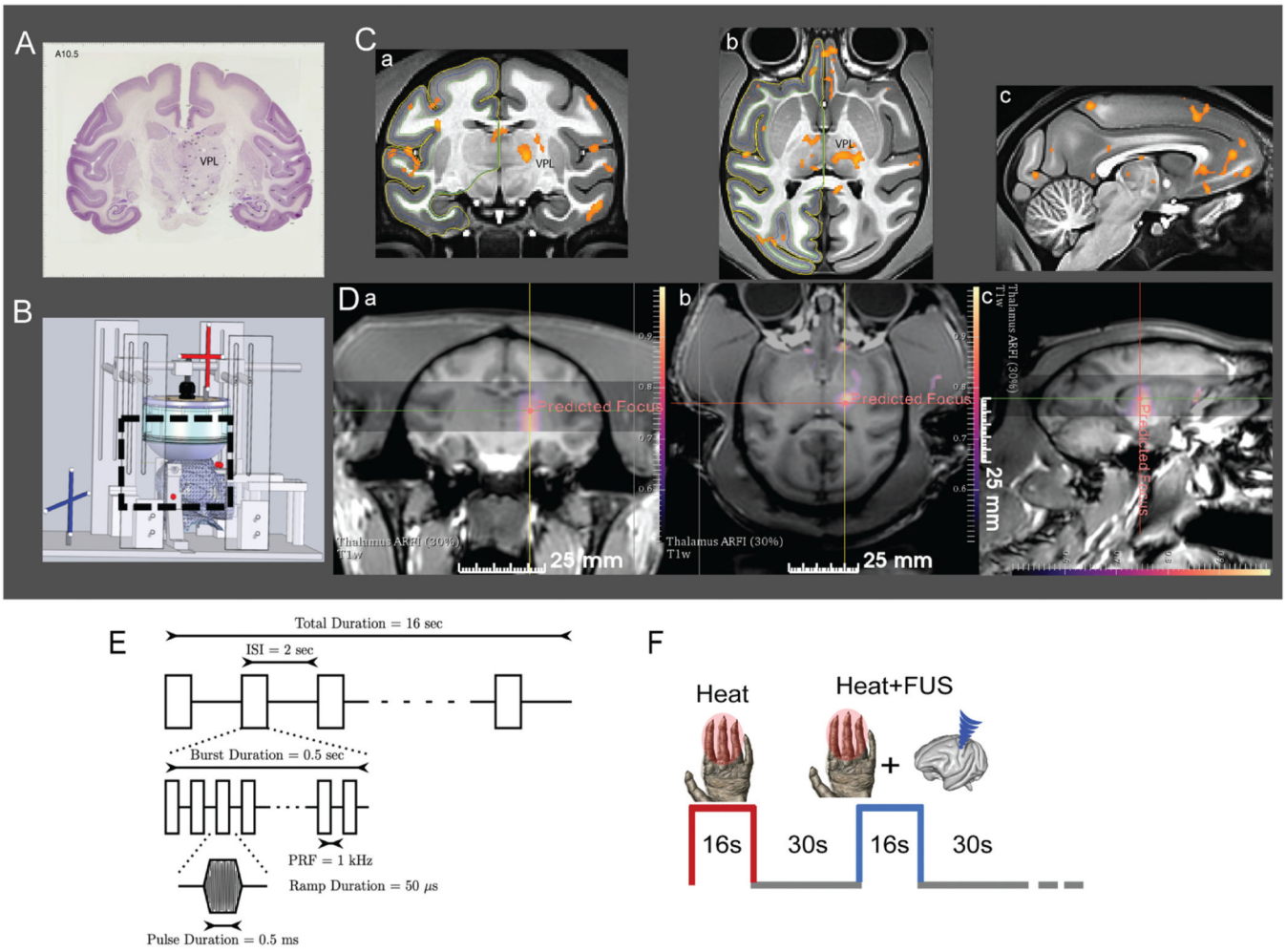

Fig. 1.

Targeted FUS stimulation of thalamus VPL nucleus with MR-ARFI feedback and fMRI monitoring. (A) Coronal section of the macaque brain with Nissl stain (adopted from brainmaps.org) shows the location of VPL nucleus. (B) Schematic showing MRI compatible stereotaxic positioning system used for experiments to place the acoustic focus at the target. (C) Coronal (a), axial (b) and sagittal (c) views of nociceptive heat (47.5 °C) stimulus-evoked fMRI activation foci. Activation foci are displayed on NMT2.0 template ($t > 2$, $p < 0.05$, FDR corrected). (D) Display of MR-ARFI focuses targeted at thalamic nuclei on coronal, axial and sagittal planes. Color scale: tissue displacement in microns. (E) A 128 channel FUS array delivered 650 kHz pulsed US with fast PRF of 1 kHz with a 50% duty cycle for 500 ms, slow PRF of 0.5 Hz for 16s. Estimated *in vivo* pressure was 550 kPa (39% transmission estimate). (F) Interleaved heat and heat + FUS stimulation presentation paradigm. (For interpretation of the references to color in this figure legend, the reader is referred to the Web version of this article.)

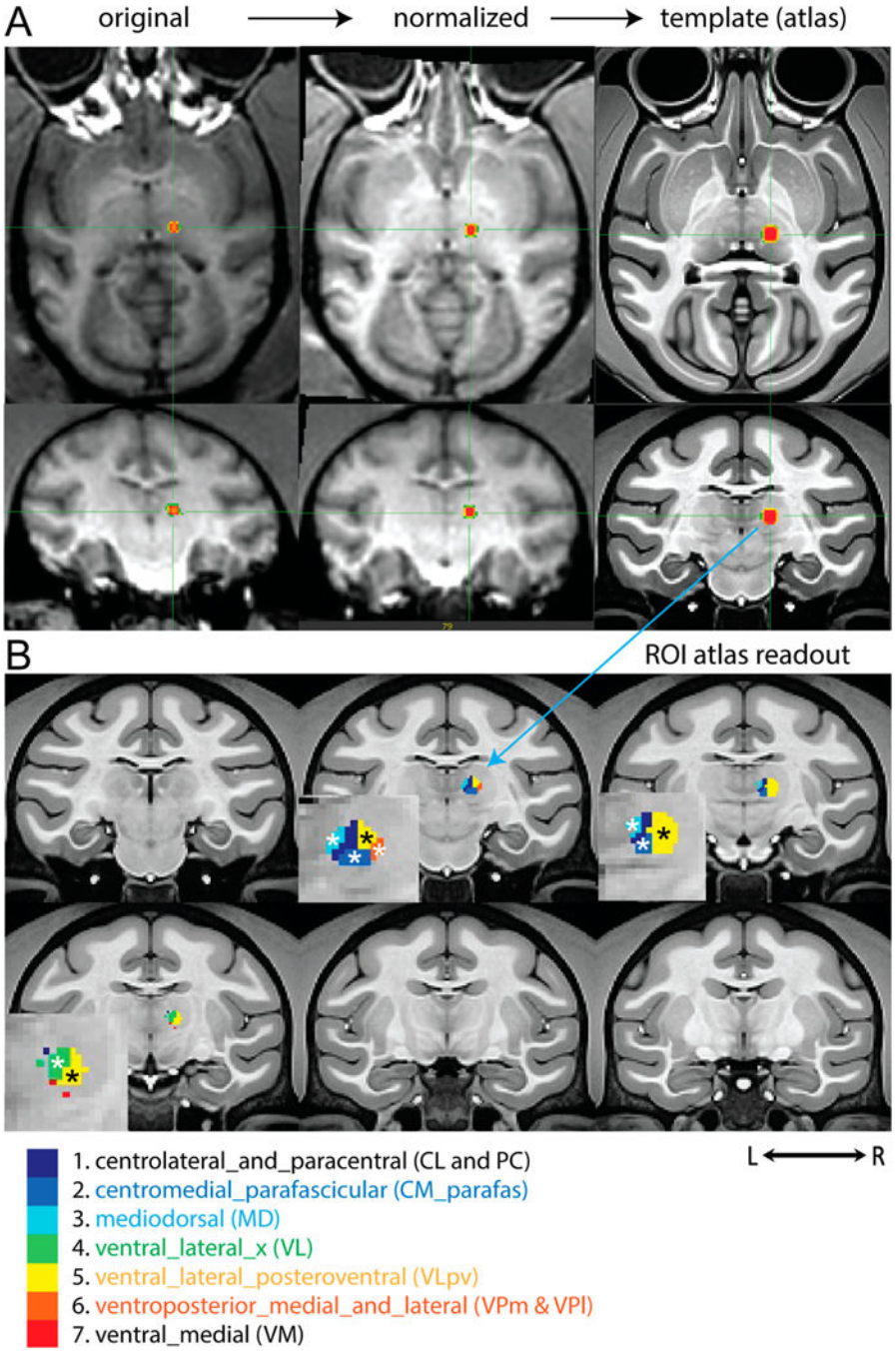

Fig. 2.

Annotation of MR-ARFI target in one representative subject. A: Steps involved in transforming MR-ARFI focus on axial and coronal images from the individual subject space (original) and then normalized to the NHP template space. B: Thalamic nuclei that were covered by ARFI focus and were stimulated by FUS. * Indicates thalamic nuclei exhibited heat-evoked BOLD activation.

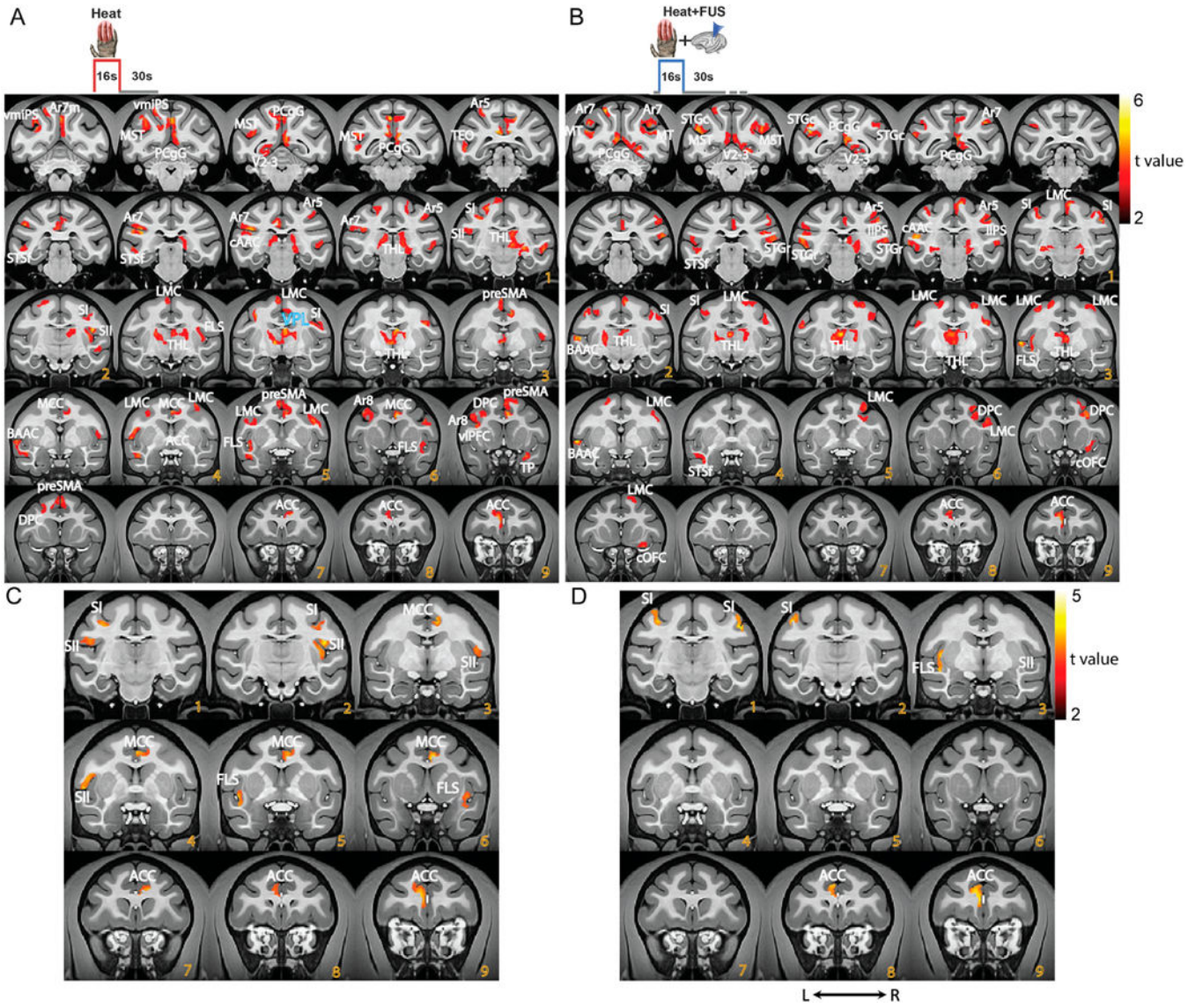

Fig. 3.

Group level nociceptive heat and heat + FUS stimulation evoked fMRI activation maps. (A, B) Stimulus (heat or heat + FUS) evoked activation t-maps overlaid on representative coronal images (NMT2.0 template). The t-maps were thresholded at $t > 2$, $p < 0.05$, and FDR corrected. Color bars present the t value ranges. (C, D) Displays thresholded t value activation maps of five selected ROIs (ACC, MCC, SI, SII and Insula (FSL)) under heat (A) and heat + FUS (C) stimulation conditions. (For interpretation of the references to color in this figure legend, the reader is referred to the Web version of this article.)

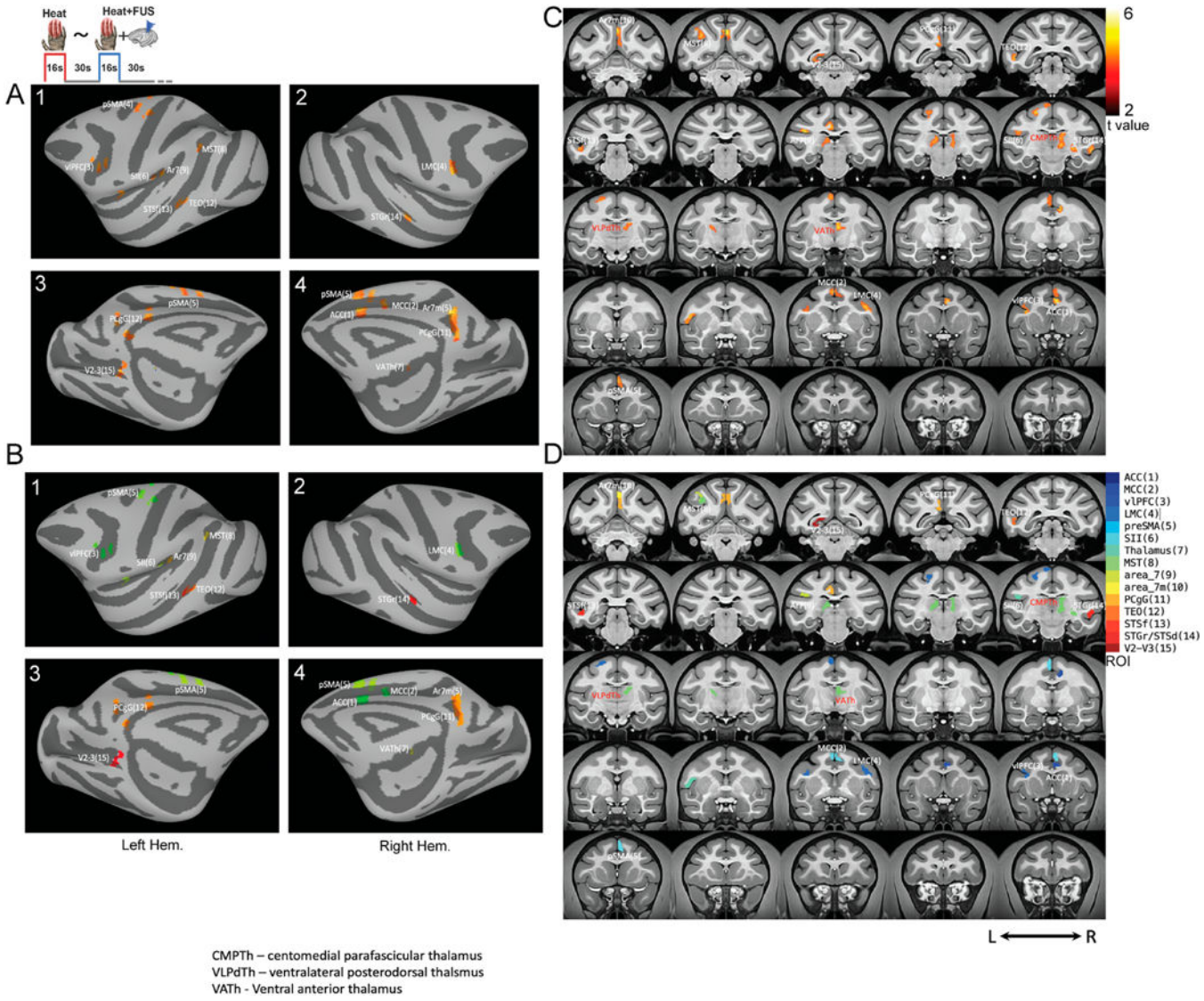

Fig. 4.

Differential fMRI activation map between heat versus heat + FUS stimulation. (A) Subtraction map of heat and heat + FUS overlaid on the inflated anatomic template (NMT2.0). A1&2 shows the lateral view of the inflated surface of the left and right hemispheres with 15 areas showing statistically significant activation ($t > 2$, $p < 0.05$, FDR corrected). A3&4 presents the medial view of the activation patterns. B1–4 refers to the color-coded ROIs on the surface. The coronal view of intensity (t-score) and color-coded ROI group activation maps are shown in C&D, respectively. Each color refers to a functionally activated ROI (Table 1) overlaid on the surface map. (For interpretation of the references to color in this figure legend, the reader is referred to the Web version of this article.)

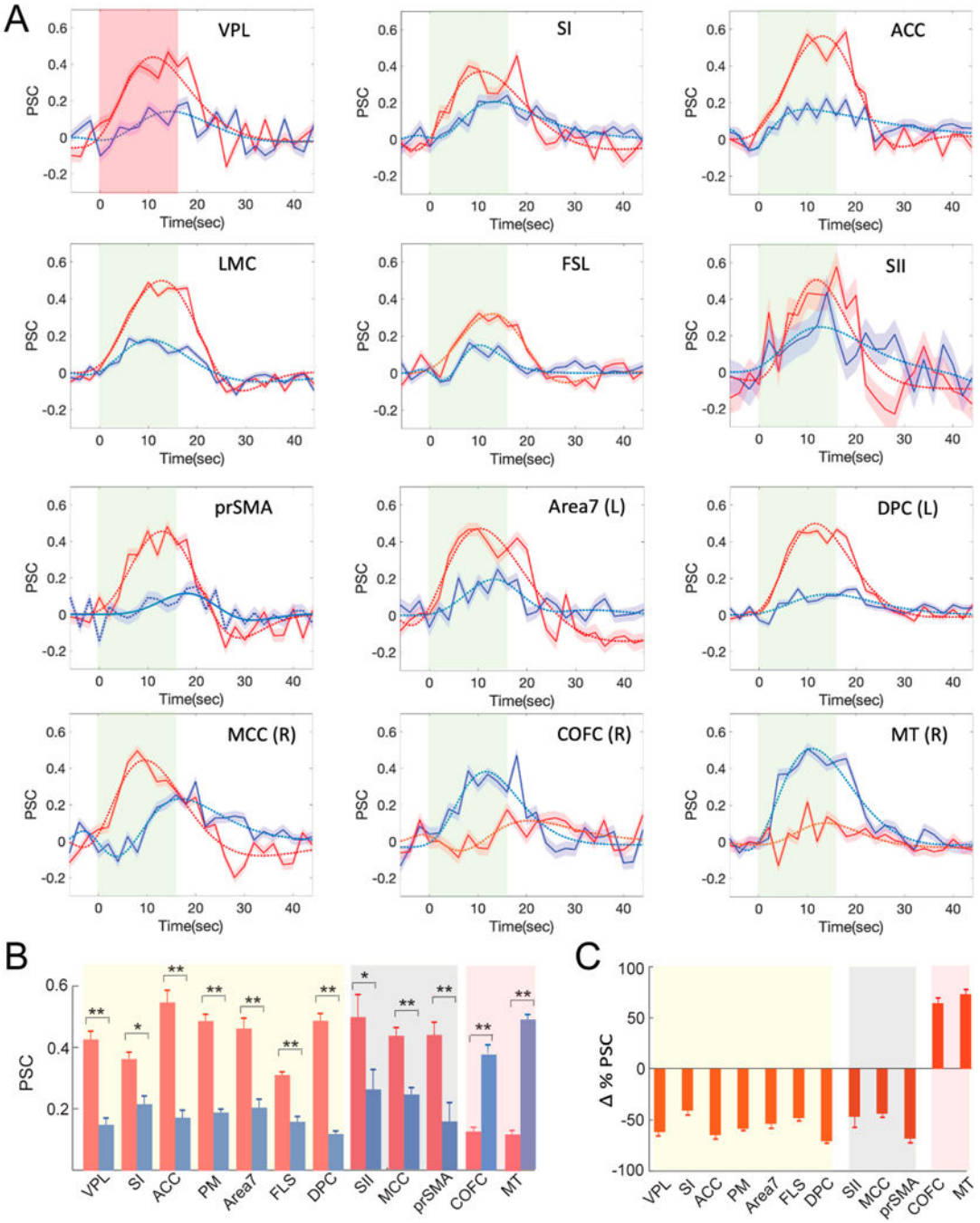

Fig. 5.

Percentage signal change (PSC) during Heat versus Heat + FUS conditions in ten representative brain regions. (A) Stimulus block averaged time courses of PSC (solid lines; mean ± standard error (SE)) extracted from voxels showing statistically significant activation ($t > 2$, $p < 0.05$, FDR corrected) within the thalamus (VPL) and representative cortical areas. Panels 1–7: jointly appeared in both stimulus conditions (heat and heat + FUS) activation maps. 8–10: showed suppression when FUS was concurrently applied. 11–12: showed strong response during heat + FUS condition. The dotted lines show the double

gamma fitting curves. Line shadow indicates SE. (B) Bar graph of the peaks of PSC in each area (mean ± SE; heat: red; heat + FUS: blue) MWW test (* < 0.05 and ** < 0.005). (C) Percentage signal changes (mean ± SE at each ROI) between heat versus heat + FUS conditions. (For interpretation of the references to color in this figure legend, the reader is referred to the Web version of this article.)

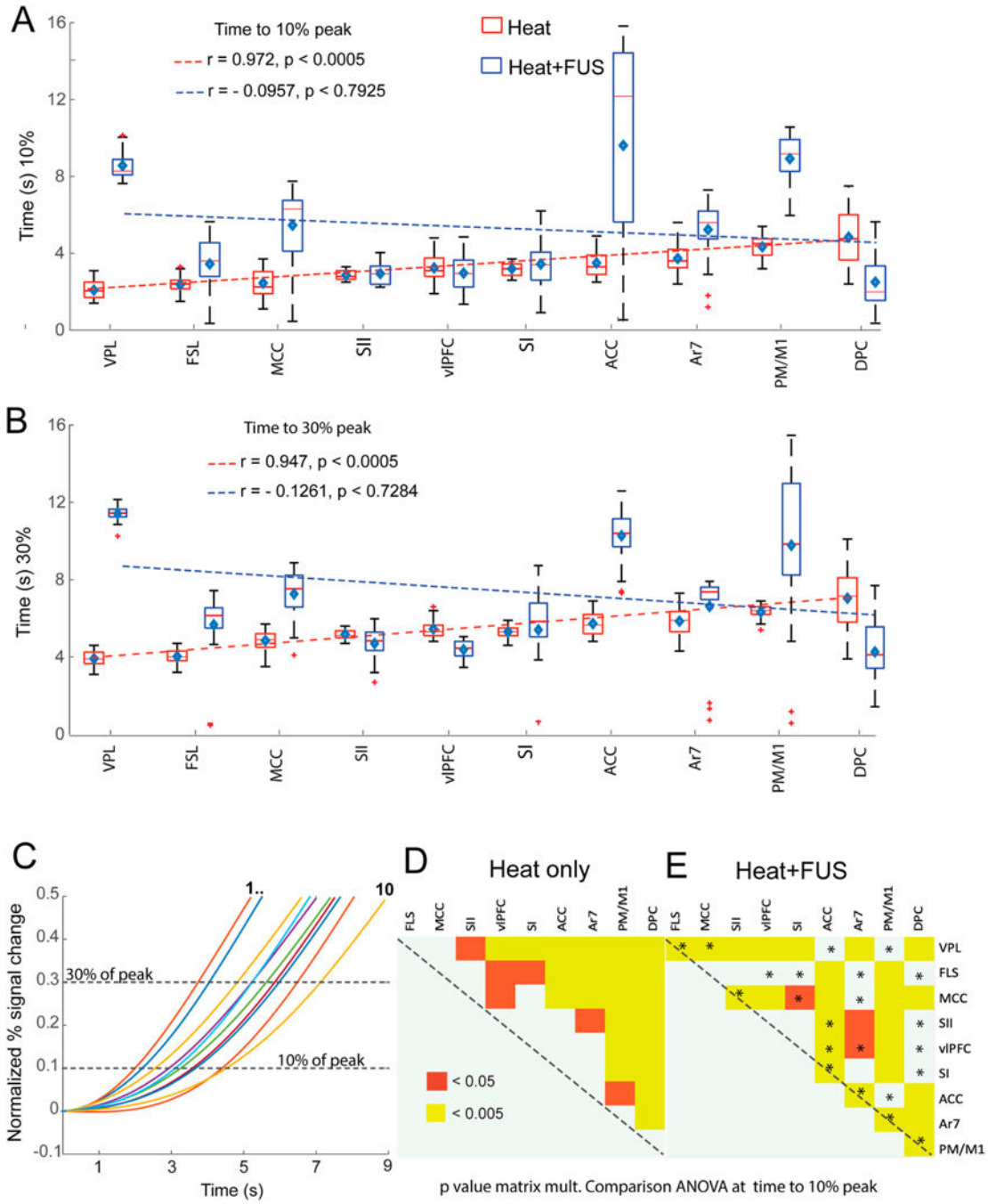

Fig. 6.

Effect of FUS on response latency and inter-regional order. (A–B) Whisker boxplots of time to reach 10% (A) and 30% (B) of the peak PSC for heat (red) and heat + FUS (blue) stimulus conditions. The brain regions are arranged in ascending order of latencies observed with heat stimulation along the x-axis. The dotted blue and red lines refer to the fitting of the median time across brain regions under heat (red) and heat + FUS (blue), respectively. The diamond symbol and short horizontal red bar indicate the median and mean time to reach 10/30% of the pick signal in each region. Pearson's product-moment correlation of

the median response time and corresponding p-values are shown in each panel. (C) Plot of the normalized percentage signal change as a function of time (post-stimulus onset) shows the signal latency to reach 10% and 30% of the peak magnitudes (dotted horizontal lines) in each brain region. Colored lines refer to fitted BOLD PSC time courses arranged in the ROI order displayed in A&B. (D&E) Matrix plots show the statistically significant differences in response time ($p < 0.05$ & 0.005) measured across ROIs to reach 10% of peak value in the heat (D) and heat + FUS (E) conditions using one-way ANOVA after multiple comparisons. (For interpretation of the references to color in this figure legend, the reader is referred to the Web version of this article.)

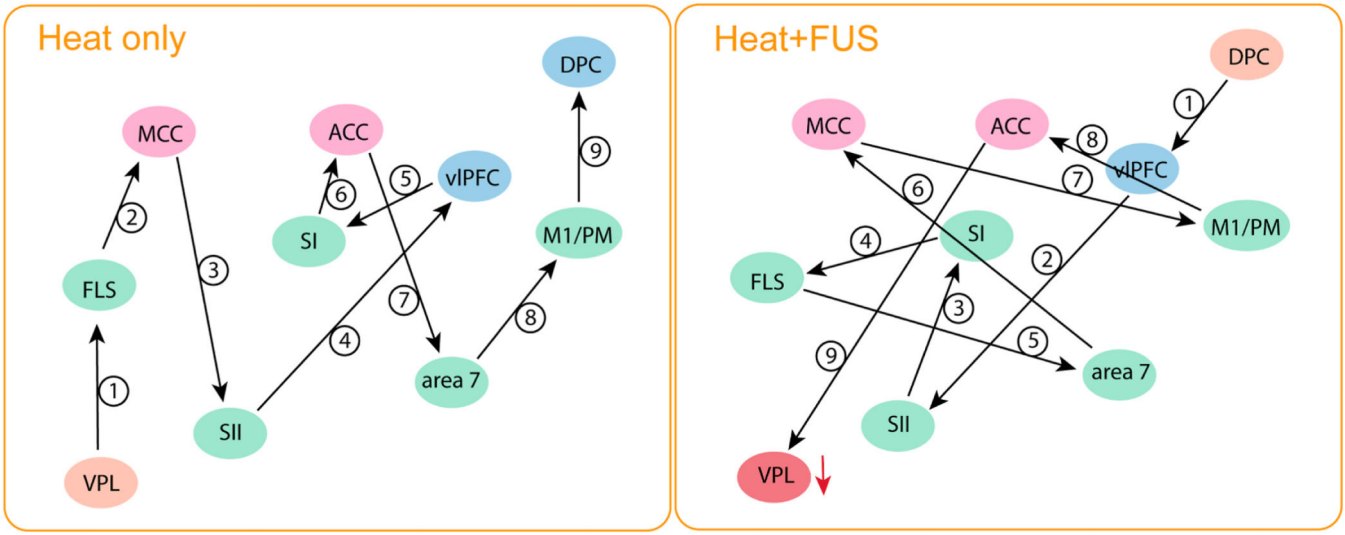

Fig. 7.

Schematic summary of information processing flow disruption during suppression of thalamic VPL heat response. SI: primary somatosensory cortex, SII: secondary somatosensory cortex, FLS: floor of lateral sulcus, M1/PM: primary and pre-motor cortex, MCC & ACC: Midcingulate and anterior cingulate cortex, vlPFC: ventrolateral prefrontal cortex, DPC: dorsolateral prefrontal cortex.

Table 1

Descriptive comparison of detected heat evoked BOLD fMRI activation due to heat, with and without FUS suppression of thalamic nuclei (VPL). The letters in blue font represent the brain regions that responded to heat under both stimulation conditions. The letter "n" denotes brain regions that exhibited non-significant signal changes in both hemispheres and '−' refers to unilateral activation. Areas displayed in red font (outline in lines 25–28) refer to additional activations detected when FUS was delivered; these were not part of the heat network (outlined in lines 1–24). The mean p-value, derived from multivariate GLM analysis of the voxels within each ROI in each hemisphere (L: left; R: right), highlighted significant responses to stimuli (with t values > 2, post-correction). These p values are presented side by side as the stimulus was presented to the left hand.

Sl	ROIs	Heat vs. rest (p Value)		Heat + FUS vs. rest (p Value)	
		L	R	L	R
1	Anterior cingulate cortex (ACC)	0.0470	0.0309	0.0382	–
2	Midcingulate cortex (MCC)	–	0.0324	n	n
3	Area8A periarcuate (Ar8A)	0.0317	–	n	n
4	Dorsolateral prefrontal cortex (DPC)	0.0412	–	–	0.0268
5	Ventrolateral prefrontal cortex (vlPFC)	0.0344	–	n	n
6	M1/PM lateral motor cortex (LMC)	0.0326	0.0401	0.0339	0.0362
7	Pre-medial supplementary motor areas (preSMA)	0.0411	0.0321	n	n
8	Primary somatosensory cortex (SI)	0.0309	0.0266	–	0.0391
9	Secondary somatosensory cortex (SII)	0.0224	0.0260	n	n
10	Area5 (Ar5)	0.0285	0.0433	0.0374	0.0325
11	Ventral posterior lateral nucleus (VPL)	0.0274	0.0364	0.0321	0.0293
12	Ventromedial intraparietal sulcus (vmIPS)	0.0286	–	n	n
13	Medial superior temporal area (MST)	0.0279	–	0.0334	0.0439
14	Area7 in the inferior parietal lobule (Ar7)	0.0308	–	0.0312	0.0398
15	Area7m on the medial wall (Ar7m)	–	0.0291	n	n
16	Posterior cingulate gyrus (PCgG)	0.0319	0.0301	0.0362	0.0396
17	TG temporal pole (TP)	–	0.0362	n	n
18	TEO area TEO (TEO)	0.0158	–	n	n
19	Fundus of the superior temporal sulcus (STSf)	0.0291	–	0.0380	–
20	Rostral superior temporal region (STGr)	0.0317	0.0364	0.0363	0.0359
21	Belt areas of auditory cortex (BAAC)	0.0302	–	0.0089	–
22	Core areas of auditory cortex (cAAC)	0.0350	–	0.0396	0.0368
23	Floor of lateral sulcus (FSL, Insula + paraInsula)	0.0377	0.0284	0.0290	–
24	V2–V3 preoccipital visual areas 2–3 (V2–3)	0.0326	–	–	0.0472
25	Caudal orbital frontal cortex (COFC)			–	0.0383
26	Lateral intraparietal sulcus (lIPS)			–	0.0457
27	Caudal superior temporal gyrus (STGc)			0.0319	0.0416
28	Middle temporal area (MT)			–	0.0404